

Quenching of g_A deduced from the β -spectrum shape of ^{113}Cd measured with the COBRA experiment

Lucas Bodenstein-Dresler,¹ Yingjie Chu,² Daniel Gehre,² Claus Gößling,¹ Arne Heimbald,² Christian Herrmann,¹ Rastislav Hodak,³ Joel Kostensalo,⁴ Kevin Kröniger,¹ Julia Küttler,² Christian Nitsch,¹ Thomas Quante,¹ Ekaterina Rukhadze,³ Ivan Stekl,³ Jouni Suhonen,⁴ Jan Tebrügge,¹ Robert Temminghoff,¹ Juliane Volkmer,² Stefan Zatschler,^{2,*} and Kai Zuber^{2,†}

¹*TU Dortmund, Lehrstuhl für Experimentelle Physik IV, Otto-Hahn-Str. 4a, 44221 Dortmund, Germany*

²*TU Dresden, Institut für Kern- und Teilchenphysik, Zellescher Weg 19, 01069 Dresden, Germany*

³*CTU Prague, Institute of Experimental and Applied Physics, CZ-12800 Prague, Czech Republic*

⁴*University of Jyväskylä, Department of Physics, P.O. Box 35, FI-40014, Finland*

(Dated: December 14, 2024)

A first dedicated measurement of the quenching of the weak axial-vector coupling strength g_A was performed by the COBRA collaboration. The β -electron spectrum shape of the fourfold forbidden non-unique decay of ^{113}Cd strongly depends on the effective value of g_A . Using an array of CdZnTe semiconductor detectors, 45 independent spectra were obtained and interpreted in the context of three different nuclear models. The resulting effective mean values are $\bar{g}_A(\text{ISM}) = 0.915 \pm 0.021$, $\bar{g}_A(\text{MQPM}) = 0.911 \pm 0.009$ and $\bar{g}_A(\text{IBFM-2}) = 0.943 \pm 0.090$. The measurement proves that the weak axial-vector constant in nuclei deviates significantly from the free value.

I. INTRODUCTION

Neutrinoless double beta ($0\nu\beta\beta$) decay is currently the only practical means of accessing the Majorana nature of the neutrino. The occurrence of $0\nu\beta\beta$ -decay requires the violation of lepton number and a non-vanishing neutrino mass. There is a host of different possible mechanisms which mediate the decay [1]. $0\nu\beta\beta$ -decay is related to the nuclear structure via the nuclear matrix elements (NMEs), calculated in many different theory frameworks (see the reviews [2–5]). An accurate calculation of the NMEs is essential for the extraction of, e.g., the Majorana neutrino mass from the (possibly) measured $0\nu\beta\beta$ half-lives. In fact, the search for $0\nu\beta\beta$ -decay is driven by experiments and their sensitivity to the beyond-the-Standard-Model physics is tied to the values of the NMEs. Even more so, the sensitivity of the present and future $0\nu\beta\beta$ -experiments depends on the value of the weak axial-vector coupling strength g_A [6]. The effective value of g_A can be considerably quenched at least in the low-energy single- β and two-neutrino double beta ($2\nu\beta\beta$) decays [7–15] (for a recent review see [16]). The quenching of g_A affects the sensitivities of the present and future $0\nu\beta\beta$ -decay experiments [6]. The presently running experiments include GERDA [17] and Majorana [18] (^{76}Ge), NEMO-3 [19–22] (^{82}Se , ^{96}Zr , ^{100}Mo , ^{116}Cd), COBRA [23] (^{116}Cd), CUORE [24] (^{130}Te), EXO [25] and KamLAND-Zen [26] (^{136}Xe), and the future experiments include LEGEND [27] (^{76}Ge), SuperNEMO [28], AMoRE [29] and LUMINEU [30] (^{100}Mo), MOON [31] (^{82}Se , ^{100}Mo), AURORA [32] (^{116}Cd), SNO+ [33] and CUPID [34] (^{130}Te), NEXT [35] and PandaX-III [36] (^{136}Xe).

Since $0\nu\beta\beta$ -decay is a high-momentum-exchange process (roughly 100 MeV) it is not clear how the results obtained for the quenching of g_A in the low-momentum-exchange β - and $2\nu\beta\beta$ -decays can be translated to $0\nu\beta\beta$ -decay. Nevertheless, the conversion from the potentially measured $0\nu\beta\beta$ -decay half-life into a Majorana neutrino mass has a g_A^4 dependence due to the involved NMEs. This is why it is important to study the quenching of g_A in as many ways as possible, even in the low-energy processes, like β -decays.

The shape functions of forbidden non-unique β -decays are complicated combinations of different NMEs and phase-space factors [37]. Moreover, their dependence on the weak coupling strengths g_V (vector part) and g_A (axial-vector part) is very non-trivial. In fact, the shape factor $C(w_e)$ can be decomposed into vector, axial-vector and mixed vector-axial-vector parts in the form [38]

$$C(w_e) = g_V^2 C_V(w_e) + g_A^2 C_A(w_e) + g_V g_A C_{VA}(w_e). \quad (1)$$

In Ref. [38] it was proposed that the shapes of β -electron spectra could be used to determine the values of the weak coupling strengths by comparing the shape of the computed spectrum with the measured one for forbidden non-unique β -decays. This method was coined the spectrum-shape method (SSM). In this study also the next-to-leading-order corrections to the β -decay shape factor were included. In the same reference the β -electron spectra were studied for the fourfold forbidden non-unique ground-state-to-ground-state β^- -decay branches $^{113}\text{Cd}(1/2^+) \rightarrow ^{113}\text{In}(9/2^+)$ and $^{115}\text{In}(9/2^+) \rightarrow ^{115}\text{Sn}(1/2^+)$ using the microscopic quasiparticle-phonon model (MQPM) [39] and the interacting shell model (ISM). The results for the ^{113}Cd decay could be compared with the experimental spectrum shape measured by Belli *et al.* [40]. The work of [38] was extended in [41] to include an interpretation in a

* stefan.zatschler@tu-dresden.de

† kai.zuber@tu-dresden.de

third nuclear model, the microscopic interacting boson-fermion model (IBFM-2) [42]. It was noticed that the β -spectrum shapes of both transitions are highly sensitive to the values of g_V and g_A , and hence a comparison of the calculated spectrum with the measured one opens a way to determine the values of these coupling strengths. It was also noticed that the predicted effective values of g_A are pretty much independent of the nuclear model, the parameters of the model Hamiltonians and the details of the underlying mean field. The studies [38, 41] were continued by the works [43] and [44] where the evolution of the β -spectra with changing value of g_A was followed for a number of highly-forbidden β^- -decays of odd- A nuclei (MQPM and ISM calculations) and even- A nuclei (ISM calculations).

In the present article we report on the measurement of the β -electron spectrum of the transition $^{113}\text{Cd}(1/2^+) \rightarrow ^{113}\text{In}(9/2^+)$ with the COBRA demonstrator and the estimation of the effective value of g_A in the three nuclear models mentioned above.

II. EXPERIMENTAL SETUP

The COBRA collaboration searches for $\beta\beta$ -decays based on room temperature CdZnTe semiconductor detectors [45]. As $0\nu\beta\beta$ -decay is an extremely rare event, the experiment is located at the Italian Laboratori Nazionali del Gran Sasso (LNGS) shielded against cosmic rays by 1400m of rock. Currently, it comprises 64 CdZnTe coplanar-grid (CPG) semiconductor detectors arranged in four layers of 4×4 detectors. This stage of the experiment is referred to as the COBRA demonstrator [46]. Each detector has a size of about $1 \times 1 \times 1 \text{ cm}^3$ and a mass of 5.9g. The detectors are supported by a polyoxymethylene frame installed in a support structure made of electroformed copper. The setup is constantly flushed with evaporated nitrogen to suppress radon-induced background. The inner housing is surrounded by 5 cm of electroformed copper, followed by a 5 cm thick layer of ultra-low activity lead ($< 3 \text{ Bq/kg}$ of ^{210}Pb) and 15 cm of standard lead. The neutron flux inside the setup is suppressed by a layer of 7 cm borated polyethylene with 2.7 wt.% of boron. Charge-sensitive preamplifiers integrate the current pulses and convert the single-ended detector pulses into differential signals in order to minimize electronic noise during transmission. After linear amplification, the pulse shapes are digitized using 100 MHz flash analog-to-digital converters (FADCs) and written to disk. A key instrument in background suppression for COBRA is the reconstruction of the so-called interaction depth [47] and the use of pulse-shape discrimination techniques [48, 49]. The four-fold forbidden non-unique β -decay of ^{113}Cd was studied with an early predecessor of the current COBRA demonstrator [50]. The analysis resulted in a half-life of $(8.00 \pm 0.11 \text{ (stat.)} \pm 0.24 \text{ (syst.)}) \times 10^{15}$ years and a Q -value of $322.2 \pm 0.3 \text{ (stat.)} \pm 0.9 \text{ (syst.) keV}$. More recently,

the ^{113}Cd β -decay was used to investigate the demonstrator's detector stability by monitoring the average decay rate over the time scale of several years [51]. The average threshold was around 170 keV rejecting about half of the total ^{113}Cd energy range. Following this study, modifications on the hardware and software level were made to optimize the demonstrator setup for a dedicated low-threshold run and to investigate the spectral shape of the β -electron spectrum with high efficiency.

III. DATA-TAKING AND EVENT SELECTION

A. Run preparation

In preparation of a dedicated ^{113}Cd run, the potential of optimizing the COBRA demonstrator towards minimum threshold operation was studied in detail. The major improvement was achieved by exchanging the coolant in the cooling system of the pre-amplifier stage which allows operation at lower temperatures. The direct cooling of the first stage of the electronics dramatically reduces the thermal component of the signal noise while at the same time the detector performance benefits from an ambient temperature slightly below room temperature. The temperature inside the inner shield of the experiment is monitored by several sensors at different positions. The optimal temperature was found to be around 9°C measured on top of the lead castle housing the detectors [46]. The detectors themselves are not cooled directly, but through convection and radiation cooling they are kept at the same temperature as the surrounding shielding components. After reaching thermal equilibrium, the optimal trigger threshold for each channel was estimated. This was done by monitoring the average trigger rate on a daily basis and adjusting the individual thresholds accordingly. The worst-performing detector channels were switched off completely for the entire ^{113}Cd run to prevent potential sources of electromagnetic interferences and crosstalk. The resulting average threshold was 83.9 keV, where the 18 best detectors were operated below or around 70 keV and the four highest at 124 keV. After reaching stable operation, the dedicated data-taking period lasted from Jul.'17 until Feb.'18.

B. Detector calibration and characterization

The energy calibration of each detector was done using the radio-nuclides ^{22}Na , ^{152}Eu and ^{228}Th providing γ -lines in the range from 121.8 keV to 2614.5 keV. Each line was fitted with a Gaussian plus a polynomial function to also describe the underlying Compton continuum. The calibration is done by a linear fit of the peak position in channel numbers versus the known γ -line energy. The full-width at half-maximum (FWHM) is parametrized as

$$\text{FWHM}(E) = \sqrt{p_0 + p_1 \cdot E + p_2 \cdot E^2}, \quad p_i > 0. \quad (2)$$

The parameter p_0 is independent of the deposited energy and accounts for a constant contribution from noise. The second term scales with \sqrt{E} and is motivated by the Poisson fluctuations of the charge carrier production while the third term is a rather small correction for CPG effects. The achieved relative resolution $\text{FWHM}(E)/E$ ranges from 7.2–21.4% at 121.8 keV with a mean value of 12.5% up to 0.9–4.6% at 2614.5 keV and a mean of 1.7%.

C. Detector selection and data quality

To ensure stable operation during the dedicated ^{113}Cd run, only data from a subset of the 64 installed detectors was selected. Three detectors suffer from problems with the data acquisition electronics or unreliable contacting and were excluded from the data-taking. In addition, twelve detectors that had to be operated with a threshold higher than 200 keV were switched off. Four additional detectors did not pass the quality requirements set for this analysis by evaluating the pre- and post-calibration data. The final detector pool for the ^{113}Cd run thus comprises 45 detectors. An average of 1.10 kg days of exposure was accumulated per detector, whereas two detectors were partly disabled and feature a reduced exposure of 0.29 kg days and 0.79 kg days, respectively. With a fraction of 5.5% of the detector mass, the combined isotopic exposure of all selected detectors for ^{113}Cd is 2.73 kg days.

D. Event selection

The standard COBRA selection cuts are used in the ^{113}Cd analysis [52]. The first stage consists of a set of data-cleaning cuts (DCCs) to remove distorted and unphysical events. The validity of those cuts was checked with a special run. In this run, all channels of the same FADCs were read out if the trigger condition was fulfilled. The triggered event trace was then rejected and only the remaining baseline pulses were analyzed. Those pulses are treated as a proxy for noise-only signals. It was found that 99.84% of the untriggered events are rejected by the DCCs with no significant difference between the detectors. The DCCs also include a mild cut on the interaction depth z to remove reconstruction artifacts near the anode side at $z = 0$. The interaction depth is further restricted to remove events with an unphysically high depth, where the planar cathode surface is located at $z = 1.0$. The depth selection is optimized for each detector individually and covers for the most part the range $0.2 < z \leq 0.97$. Lastly, coincidences between neighboring detectors of the same FADC are rejected. No further pulse-shape discrimination cuts are necessary since the ^{113}Cd decay is by far the strongest signal for COBRA at low energies.

E. Background description

Above the ^{113}Cd Q -value of 322.2 keV, the measured count rate drops by at least two orders of magnitude. The maximum count rate for the average ^{113}Cd spectrum of all detectors is about 175 cts/(kg keV d) at 150 keV and drops sharply to below 1.5 cts/(kg keV d) at 330 keV. The background decreases exponentially for higher energies with only a few characteristic features. At even higher energies two α -decay peaks are present originating from ^{190}Pt ($Q_\alpha = 3.2$ MeV) and ^{210}Po ($Q_\alpha = 5.4$ MeV). Platinum is part of the electrode metalization while ^{210}Po is a daughter nucleus of the natural radon decay chain. Both event populations are removed completely by a cut on the interaction depth due to their localized origin on the cathode side. In the most recent $0\nu\beta\beta$ -decay search the background index for the ^{116}Cd region of interest is quoted with 2.7 cts/(kg keV yr) [52]. The remaining background is expected to be dominated by α -decays on the lateral surfaces. The α -particles have to pass through the encapsulation lacquer of the detector of about 100 μm thickness before they can deposit energy in the sensitive volume. Because of the inhomogeneity of the lacquer the energy spectrum is strongly deteriorated with no noticeable peak position. In the combined spectrum of the dedicated ^{113}Cd run there is no clear hint for the annihilation line at 511 keV or the γ -lines of primordial radio-nuclei such as ^{40}K or the natural decay chains of uranium and thorium. Instead, there is an indication for two new γ -lines at 351.9 keV and 609.3 keV. These lines originate from the decays of ^{214}Pb and ^{214}Bi as short-living ^{222}Rn daughters and correspond to the dominant de-excitation processes. In Dec.'17 there was a short period without nitrogen flushing of the inner shield of the experiment causing this radon exposure. Furthermore, there is no sign for a contribution of the ^{113m}Cd β -decay with a Q -value of 585.7 keV as considered in Ref. [40]. An increased analysis threshold with respect to the original trigger threshold ensures that there is no noise contribution leaking into the signal region at low energies. The average ratio of the exposure weighted integral over the ^{113}Cd region of interest and the total integral is 99.82%. Because of the overwhelming dominance of the ^{113}Cd decay at low energies and the absence of clear background indications, no background is considered in the spectral shape analysis.

IV. ANALYSIS

A. Preparation of templates

The energy spectra are compared to a set of ^{113}Cd template spectra calculated for different nuclear models in dependence of the weak axial-vector coupling strength g_A . The calculations have been carried out for $g_A \in [0.8, 1.3]$ in 0.05 steps with an energy binning of about 1 keV and in steps of 0.01 in the range of

[0.85, 1.00]. The upper bound of the range is motivated by the free value $g_A^{\text{free}} = 1.276(4)$ [53]. Splines are used to interpolate the bin content between different values of g_A for each energy bin. For the interpolation the *TSpline3* class of the *ROOT* software package [54] is used which utilizes polynomials of grade three. The uncertainty of this interpolation method was conservatively estimated to be below 0.2%. For the comparison with the data, the finite energy resolution and the electron detection efficiency have to be taken into account. This is done by folding the templates with the resolution function and the energy dependent detection efficiency $\varepsilon(E)$. The latter is incorporated as a scaling factor $\varepsilon(E_i)$ for each energy bin i of the templates prior to the folding with the resolution. The detection efficiency is determined from Monte Carlo simulations based on GEANT4 [55]. Finally, each template spectrum is normalized by the integral over the accessible energy range depending on the threshold of each individual detector.

B. Spectral shape comparison

As the individual detector thresholds had to be adjusted slightly over the run time of the data-taking, it is necessary to normalize each energy bin with its corresponding exposure. The binning of the data is chosen with respect to the energy resolution and fixed to 4 keV. An additional analysis threshold was added in order to ensure that near-threshold effects due to noise are not affecting the signal region. The analysis threshold was set at least 8 keV above the original one. This increases the average threshold for the final analysis to 98.5 keV. The measured spectra are normalized to unity as well.

For the actual spectral shape comparison a χ^2 test was used. Using the experimental values m_i of the energy bin i with Poisson uncertainties σ_i and the corresponding prediction t_i based on the template calculated for a certain g_A , the quantity χ^2 is derived as

$$\chi^2 = \sum_{i=1}^N \left(\frac{m_i - t_i}{\sigma_i} \right)^2. \quad (3)$$

A comparison of one of the single detector measurements and a set of interpolated ^{113}Cd ISM templates is illustrated in Fig. 1. For the same detector the reduced $\chi_{\text{red}}^2(g_A) = \chi^2(g_A)/(N - 1)$ in the given g_A range is shown in Fig. 2. The curve shows two minima with the lower one at $g_A = 0.914 \pm 0.001$, where the uncertainty is calculated from the minimum $\chi^2 + 1$ as 1σ deviation. This procedure is repeated for all of the 45 independent single detector spectra.

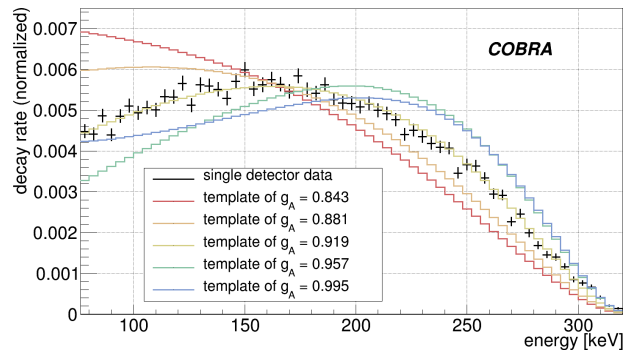


FIG. 1: Comparison of five interpolated, normalized template spectra based on the ISM calculations for the ^{113}Cd β -electron distribution and a single detector spectrum.

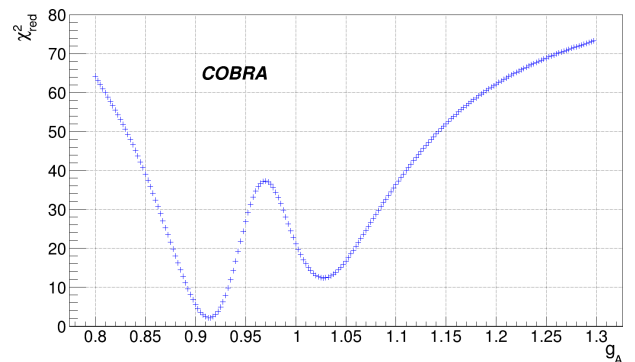


FIG. 2: χ_{red}^2 distribution for one example detector evaluated with the interpolated ISM templates.

C. Results

The resulting distribution of the best fit values for the 45 independent measurements and the three nuclear models considered is shown in Fig. 3.

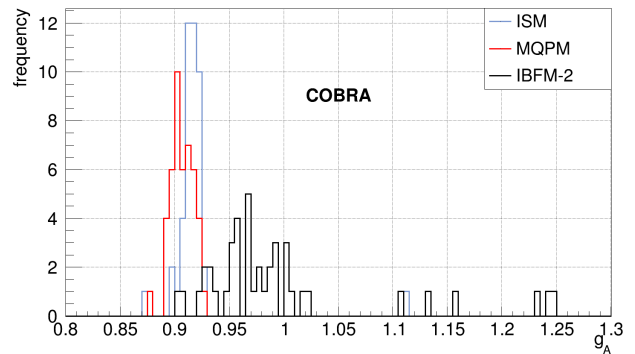


FIG. 3: Distribution of the best match g_A values for the ISM, MQPM and IBFM-2.

While the ISM and MQPM results are tightly distributed around a common mean value, the IBFM-2 distribution is much wider. This also affects the statistical uncertainty

which is quoted here as the uncertainty of the weighted mean \bar{g}_A . For the ISM and MQPM the statistical uncertainties are on the order of $2 \cdot 10^{-4}$ and a factor of four higher for IBFM-2, respectively. The overall uncertainty is dominated by the systematics and yields the following results

$$\bar{g}_A(\text{ISM}) = 0.915 \pm 0.021, \quad (4)$$

$$\bar{g}_A(\text{MQPM}) = 0.911 \pm 0.009, \quad (5)$$

$$\bar{g}_A(\text{IBFM-2}) = 0.943 \pm 0.090. \quad (6)$$

Three detector spectra could not be evaluated in the context of the IBFM-2 due to an abnormal $\chi_{\text{red}}^2(g_A)$ curve and are not considered in the final results.

D. Systematic uncertainties

The systematic uncertainties are determined after fixing all input parameters of the spectral shape analysis. Each parameter considered is varied in a defined way and the complete analysis is carried out while the other parameters are fixed to their default values. The systematic uncertainty is taken as the maximum difference between the altered and the default weighted mean. The overall systematic uncertainty for each model is obtained as the square root of the sum of squared uncertainties. A summary of the systematics is given in Tab. I.

TABLE I: Summary of systematic uncertainties.

parameter	model [%]		
	ISM	MQPM	IBFM-2
efficiency $\varepsilon(E)$	0.007	0.006	0.022
resolution FWHM(E)	0.565	0.039	3.555
calibration shift	2.231	1.010	8.830
template interpolation	0.001	0.001	0.001
χ_{red}^2 fit range	0.013	0.011	0.012
final uncertainty	2.302	1.011	9.519

The effect of the efficiency scaling is studied by changing the crystal size in the simulation to the minimum and maximum physical dimensions of the selected detectors. The systematic differences are then added in quadrature. To evaluate the influence of the resolution

smearing the FWHM(E) is fixed to the worst and best resolution curve. Following, the spectral shape analysis is repeated with fixed FWHM(E) and the systematic differences are again added in quadrature. The maximum calibration offset in the pre- and post calibration of roughly 4 keV is used to study the systematics due to a misaligned energy calibration. It turns out that this is the dominating contribution. The influence of the fit range to extract the minimum $\chi_{\text{red}}^2(g_A)$ is taken into account as another systematic uncertainty.

The total systematic uncertainties add up to a value on the percent level. The impact on the three model predictions is different due to the underlying distribution of the best match g_A values as can be seen in Fig. 3. As a consistency test, the complete analysis was repeated for two disjunct depth selections covering both halves of the detector volume. The relative difference of the resulting mean g_A compared to the full detector results (4)-(6) are 0.5% (ISM), 0.3% (MQPM) and 2.1% (IBFM-2), which is in excellent agreement with the overall uncertainties.

V. CONCLUSION

The spectral shape of the fourfold forbidden non-unique β -decay of ^{113}Cd has been investigated with 45 CdZnTe detectors and an average energy threshold of 98.5 keV. The data set corresponds to an isotopic exposure of 2.73 kg days. It was found that the COBRA data supports a significantly quenched g_A value in the low-momentum-exchange β -decay of ^{113}Cd independent of the underlying nuclear model. The ISM, MQPM and IBFM-2 results agree well within the uncertainties.

ACKNOWLEDGMENTS

We thank the LNGS for the continuous support of the COBRA experiment, and the AMANDA collaboration, especially R. Wischniewski, for providing us with their FADCs. COBRA is supported by the German Research Foundation DFG (ZU123/3 and GO1133/1) and by the Ministry of Education, Youth and Sports of the Czech Republic with Contract No. CZ.02.1.01/0.0/0.0/16_013/0001733.

-
- | | |
|--|--|
| <p>[1] J. D. Vergados, H. Ejiri, and F. Šimkovic. Neutrinoless double beta decay and neutrino mass. <i>Int. J. Mod. Phys. E</i>, 25(11):1630007, 2016.</p> <p>[2] J. Suhonen and O. Civitarese. Weak-interaction and nuclear-structure aspects of nuclear double beta decay. <i>Phys. Rep.</i>, 300(3):123 – 214, 1998.</p> <p>[3] J. Suhonen and O. Civitarese. Double-beta-decay nuclear matrix elements in the qrpq framework. <i>J. Phys. G</i>, 39(8):085105, 2012.</p> | <p>[4] J. Suhonen and O. Civitarese. Review of the properties of the $0\nu\beta^-\beta^-$ nuclear matrix elements. <i>J. Phys. G</i>, 39(12):124005, 2012.</p> <p>[5] J. Engel and J. Menéndez. Status and future of nuclear matrix elements for neutrinoless double-beta decay: a review. <i>Rep. Prog. Phys.</i>, 80(4):046301, 2017.</p> <p>[6] J. Suhonen. Impact of the quenching of g_A on the sensitivity of $0\nu\beta\beta$ experiments. <i>Phys. Rev. C</i>, 96:055501, Nov 2017.</p> |
|--|--|

- [7] A. Juodagalvis and D. J. Dean. Gamow-Teller GT_+ distributions in nuclei with mass $A = 90-97$. *Phys. Rev. C*, 72:024306, Aug 2005.
- [8] A. Faessler, G. L. Fogli, E. Lisi, V. Rodin, A. M. Rotunno, and F. Šimkovic. Overconstrained estimates of neutrinoless double beta decay within the QRPA. *J. Phys. G*, 35(7):075104, 2008.
- [9] E. Caurier, F. Nowacki, and A. Poves. Shell Model description of the $\beta\beta$ decay of ^{136}Xe . *Phys. Lett. B*, 711(1):62 – 64, 2012.
- [10] J. Suhonen and O. Civitarese. Probing the quenching of g_A by single and double beta decays. *Phys. Lett. B*, 725(1):153 – 157, 2013.
- [11] J. Suhonen and O. Civitarese. Single and double beta decays in the $A = 100$, $A = 116$ and $A = 128$ triplets of isobars. *Nucl. Phys. A*, 924:1 – 23, 2014.
- [12] H. Ejiri, N. Soukouti, and J. Suhonen. Spin-dipole nuclear matrix elements for double beta decays and astro-neutrinos. *Phys. Lett. B*, 729:27 – 32, 2014.
- [13] H. Ejiri and J. Suhonen. GT neutrino–nuclear responses for double beta decays and astro neutrinos. *J. Phys. G*, 42(5):055201, 2015.
- [14] P. Pirinen and J. Suhonen. Systematic approach to β and $2\nu\beta\beta$ decays of mass $A = 100 - 136$ nuclei. *Phys. Rev. C*, 91:054309, May 2015.
- [15] F. F. Deppisch and J. Suhonen. Statistical analysis of β decays and the effective value of g_A in the proton-neutron quasiparticle random-phase approximation framework. *Phys. Rev. C*, 94:055501, Nov 2016.
- [16] J. Suhonen. Value of the Axial-Vector Coupling Strength in β and $\beta\beta$ Decays: A Review. *Front. Phys.*, 55, 2017.
- [17] M. Agostini et al. (GERDA collaboration). Improved Limit on Neutrinoless Double- β Decay of ^{76}Ge from GERDA Phase II. *Phys. Rev. Lett.*, 120:132503, Mar 2018.
- [18] C. E. et al. (Majorana collaboration) Aalseth. Search for Neutrinoless Double- β Decay in ^{76}Ge with the Majorana Demonstrator. *Phys. Rev. Lett.*, 120:132502, Mar 2018.
- [19] R. Arnold et al. (NEMO-3 collaboration). Study of $2\nu\beta\beta$ decay of ^{100}Mo and ^{82}Se using the NEMO3 detector. *JETP Lett.*, 80(6):377–381, Sep 2004.
- [20] J. Argyriades et al. (NEMO-3 collaboration). Measurement of the two neutrino double beta decay half-life of Zr-96 with the NEMO-3 detector. *Nucl. Phys. A*, 847(3):168 – 179, 2010.
- [21] R. Arnold et al. (NEMO-3 collaboration). Results of the search for neutrinoless double- β decay in ^{100}Mo with the NEMO-3 experiment. *Phys. Rev. D*, 92:072011, Oct 2015.
- [22] R. Arnold et al. (NEMO-3 collaboration). Measurement of the $2\nu\beta\beta$ decay half-life and search for the $0\nu\beta\beta$ decay of ^{116}Cd with the NEMO-3 detector. *Phys. Rev. D*, 95:012007, Jan 2017.
- [23] S. Zatschler (COBRA collaboration). The COBRA experiment – Status and prospects on the search of neutrinoless double beta-decay. *AIP Conf. Proc.*, 1686(1):020027, 2015.
- [24] C. Alduino et al. (CUORE collaboration). First Results from CUORE: A Search for Lepton Number Violation via $0\nu\beta\beta$ Decay of ^{130}Te . *Phys. Rev. Lett.*, 120:132501, Mar 2018.
- [25] J. B. Albert et al. (EXO-200 collaboration). Search for Neutrinoless Double-Beta Decay with the Upgraded EXO-200 Detector. *Phys. Rev. Lett.*, 120:072701, Feb 2018.
- [26] A. Gando et al. (KamLAND-Zen collaboration). Search for Majorana Neutrinos Near the Inverted Mass Hierarchy Region with KamLAND-Zen. *Phys. Rev. Lett.*, 117:082503, Aug 2016.
- [27] N. Abgrall et al. (LEGEND collaboration). The Large Enriched Germanium Experiment for Neutrinoless Double Beta Decay (LEGEND). In *Proceeding of the MEDEX'17 meeting (Prague)*, 2017.
- [28] R. Hodák (SuperNEMO collaboration). Status of the SuperNEMO demonstrator. *AIP Conf. Proc.*, 1686(1):020012, 2015.
- [29] H. Park (AMoRE collaboration). The AMoRE: Search for neutrinoless double beta decay of ^{100}Mo . *AIP Conf. Proc.*, 1686(1):020016, 2015.
- [30] T.B. Bekker et al. (LUMINEU collaboration). Above-ground test of an advanced Li_2MoO_4 scintillating bolometer to search for neutrinoless double beta decay of ^{100}Mo . *Astropart. Phys.*, 72:38 – 45, 2016.
- [31] K. Fushimi, Y. Kameda, K. Harada, S. Nakayama, H. Ejiri, T. Shima, K. Yasuda, R. Hazama, and K. Imagawa. Moon for double-beta decays and neutrino nuclear responses. *J. Phys. Conf. Series*, 203(1):012064, 2010.
- [32] F. A. Danevich et al. (AURORA collaboration). Search for double beta decay of ^{116}Cd with enriched $^{116}\text{CdWO}_4$ crystal scintillators (Aurora experiment). *J. Phys. Conf. Series*, 718(6):062009, 2016.
- [33] S. Andringa et al. (SNO+ collaboration). Current Status and Future Prospects of the SNO+ Experiment. *Adv. High Energy Phys.*, 2016:6194250, 2016.
- [34] D.R. Artusa et al. (CUPID collaboration). Enriched TeO_2 bolometers with active particle discrimination: Towards the CUVID experiment. *Phys. Lett. B*, 767:321 – 329, 2017.
- [35] J. Martín-Albo et al. (NEXT collaboration). Sensitivity of NEXT-100 to neutrinoless double beta decay. *J. High Energy Phys.*, 2016(5):159, May 2016.
- [36] X. Chen et al. (PandaX-III collaboration). PandaX-III: Searching for neutrinoless double beta decay with high pressure ^{136}Xe gas time projection chambers. *Sci. China Phys. Mech. Astron.*, 60(6):061011, Apr 2017.
- [37] M. T. Mustonen, M. Aunola, and J. Suhonen. Theoretical description of the fourth-forbidden non-unique β decays of ^{113}Cd and ^{115}In . *Phys. Rev. C*, 73:054301, May 2006.
- [38] M. Haaranen, P. C. Srivastava, and J. Suhonen. Forbidden nonunique β decays and effective values of weak coupling constants. *Phys. Rev. C*, 93:034308, Mar 2016.
- [39] J. Toivanen and J. Suhonen. Microscopic quasiparticle-phonon description of odd-mass $^{127-133}\text{Xe}$ isotopes and their β decay. *Phys. Rev. C*, 57:1237–1245, Mar 1998.
- [40] P. Belli et al. Investigation of β decay of ^{113}Cd . *Phys. Rev. C*, 76:064603, Dec 2007.
- [41] M. Haaranen, J. Kotila, and J. Suhonen. Spectrum-shape method and the next-to-leading-order terms of the β -decay shape factor. *Phys. Rev. C*, 95:024327, Feb 2017.
- [42] F. Iachello and P. van Isacker. *The Interacting Boson-Fermion Model*. Cambridge Monographs on Mathematical Physics. Cambridge University Press, 1991.
- [43] J. Kostensalo, M. Haaranen, and J. Suhonen. Electron spectra in forbidden β decays and the quenching of the weak axial-vector coupling constant g_A . *Phys. Rev. C*, 95:044313, Apr 2017.
- [44] J. Kostensalo and J. Suhonen. g_A -driven shapes of electron spectra of forbidden β decays in the nuclear shell

- model. *Phys. Rev. C*, 96:024317, Aug 2017.
- [45] K. Zuber. COBRA – double beta decay searches using CdTe detectors. *Phys. Lett. B*, 519(1):1 – 7, 2001.
- [46] J. Ebert et al. (COBRA collaboration). The COBRA demonstrator at the LNGS underground laboratory. *Nucl. Instrum. Methods A*, 807:114 – 120, 2016.
- [47] M. Fritts and J. Durst and T. Göpfert and T. Wester and K. Zuber. Analytical model for event reconstruction in coplanar grid CdZnTe detectors. *Nucl. Instrum. Methods A*, 708:1 – 6, 2013.
- [48] M. Fritts et al. (COBRA collaboration). Pulse-shape discrimination of surface events in CdZnTe detectors for the COBRA experiment. *Nucl. Instrum. Methods A*, 749:27 – 34, 2014.
- [49] S. Zatschler. Discrimination of single-site and multi-site events in CZT-CPG detectors for the COBRA experiment. In *2016 IEEE Nuclear Science Symposium, Medical Imaging Conference and Room-Temperature Semiconductor Detector Workshop (NSS/MIC/RTSD)*, pages 1–5, 2016.
- [50] J.V. Dawson et al. (COBRA collaboration). An investigation into the ^{113}Cd beta decay spectrum using a CdZnTe array. *Nucl. Phys. A*, 818(3):264 – 278, 2009.
- [51] J. Ebert et al. (COBRA collaboration). Long-term stability of underground operated CZT detectors based on the analysis of intrinsic ^{113}Cd β^- -decay. *Nucl. Instrum. Methods A*, 821:109 – 115, 2016.
- [52] J. Ebert et al. (COBRA collaboration). Results of a search for neutrinoless double- β decay using the COBRA demonstrator. *Phys. Rev. C*, 94:024603, Aug 2016.
- [53] J. Liu et al. (UCNA collaboration). Determination of the Axial-Vector Weak Coupling Constant with Ultracold Neutrons. *Phys. Rev. Lett.*, 105:219903, Nov 2010.
- [54] R. Brun and F. Rademakers. ROOT – An object oriented data analysis framework. *Nucl. Instrum. Methods A*, 389(1):81 – 86, 1997. Release 6.12/04 - 2017-12-13.
- [55] J. Allison et al. Recent developments in Geant4. *Nucl. Instrum. Methods A*, 835:186 – 225, 2016. Release 10.0.p04.